Electronic Supplementary Material (ESI) for Inorganic Chemistry Frontiers.

Selective Signalling of Alcohols by Molecular Lattice and Mechanism of Single-Crystal-to-Single-Crystal Transformation.

José Sánchez Costa, Santiago Rodríguez-Jiménez, Gavin A. Craig, Benjamin Barth, Christine Beavers, Simon J. Teat, Kevin Gagnon, Leoní A. Barrios, Olivier Roubeau and Guillem Aromí

Table S1. Crystallographic data for compounds **3**·EtOH, **3**·PrOH^A, **3**·PrOH^B, **3**·PrOH^C and **4**·”PrOH”.

Compound	**3**·EtOH	**3**·PrOH	**3**·PrOH^A	**3**·PrOH^B	**3**·PrOH^C	**4**·”PrOH”
T (K)	250	100	100	100	100	100
Formula	$C_{39}H_{40}Cl_2$ $Fe\ N_{10}O_{12}$		$C_{39}H_{38}Cl_2$ $FeN_{10}O_{11}$	$C_{38.62}H_{37}Cl_2$ $FeN_{10}O_{10.88}$	$C_{37.05}H_{32.80}Cl_2$ $FeN_{10}O_{10.35}$	$C_{39}H_{40}Cl_2$ $Fe\ N_{10}O_{12}$
FW (g mol^{-1})	967.56		949.54	942.03	910.48	889.45
λ (Å)	0.7749	0.71073	0.7749	0.7749	0.7749	0.7749
crystal system	triclinic	triclinic	triclinic	triclinic	triclinic	triclinic
space group	$P\bar{1}$	$P\bar{1}$	$P\bar{1}$	$P\bar{1}$	$P\bar{1}$	$P\bar{1}$
a (Å)	12.790(4)	11.203(3)	11.1233(5)	11.2961(4)	10.8268(6)	10.5958(4)
b (Å)	13.158(4)	11.960(2)	11.9616(5)	12.0540(4)	11.9498(6)	11.8395(4)
c (Å)	15.054(5)	16.983(4)	16.9794(7)	17.1342(5)	17.0106(7)	17.0521(5)
α (º)	71.548(4)	100.583(16)	100.602(2)	100.716(2)	100.463(3)	101.136(2)
β (º)	69.217(4)	106.105(16)	105.946(2)	107.7683(19)	106.141(3)	105.917(2)
γ (º)	63.267(4)	108.045(15)	107.618(2)	108.3975(19)	107.590(3)	106.551(2)
V (Å^3)	2077.7(11)	1986.1(8)	1980.42(15)	2002.72(12)	1928.55(17)	1884.61(12)
Z	2		2	2	2	2
ρ_{calcd} (g cm^{-3})	1.547		1.592	1.562	1.568	1.567
μ (mm^{-1})	0.713		0.744	0.735	0.758	0.773
Reflections	5983		16425	12234	5015	4597
R_{int}	0.0520		0.0607	0.0623	0.0684	0.0486
Parameters	592		585	632	669	580
Restraints	225		5	245	586	350
*R*1 [$I > 2\sigma(I)$]	0.0653		0.0564	0.0611	0.0787	0.0740
*wR*2 [$I > 2\sigma(I)$]	0.1600		0.1380	0.1562	0.1773	0.1938
*R*1 [all]	0.0946		0.0931	0.0947	0.1135	0.0997
*wR*2 [all]	0.1865		0.1558	0.1730	0.1949	0.2161
S	1.072		1.040	1.033	1.073	1.043
Largest peak / hole (*e* Å^3)	0.765 / –0.595		1.195 / –0.648	1.238 / –0.691	0.895 / –0.575	0.929 / –0.495
avg. Fe-N (Å)	1.94(3)		1.951(9)	1.956(12)	1.95(4)	1.95(3)

Table S2. Details of hydrogen bonds in the structures of **3**·EtOH, **3**·PrOH^{A}, **3**·PrOH^{B}, **3**·PrOH^{C} and **4**·”PrOH”.

	D–H	H···A	D···A	D–H···A
		3·EtOH		
N1–H1A···O1	0.87	1.99	2.593(8)	125.3
N5–H5···O1_2	0.87	2.04	2.874(7)	160.5
N6–H6A···O1S	0.87	1.89	2.739(9)	165.8
N10–H10···O3	0.87	2.02	2.889(10)	178.1
N10–H10···O4	0.87	2.07	2.94(5)	171.3
O1S–H1S···O2W	0.83	1.90	2.619(12)	144.7
		3·PrOH^{A}		
N1–H1D···O9	0.87(2)	2.10(3)	2.609(2)	116(2)
N5–H5B···O1S	0.89(2)	1.98(2)	2.864(3)	172(3)
N6–H6B···O2	0.839(17)	2.010(17)	2.848(3)	177(3)
N10–H10A···O5	0.862(17)	1.914(17)	2.774(2)	174(3)
O1S–H1S···O1	0.95(3)	1.89(3)	2.783(3)	155(3)
		3·PrOH^{B}		
N1–H1A···O9	0.884(18)	2.10(3)	2.622(3)	117(3)
N5–H5B···O1S	0.887(18)	1.97(2)	2.832(4)	164(3)
N6–H6B···O2	0.893(18)	1.82(4)	2.67(2)	159(3)
N10–H10A···O5	0.904(18)	1.894(19)	2.796(3)	175(3)
O1S–H1S···O1	0.883(19)	1.86(4)	2.72(3)	163(4)
O1S–H1S···O1A	0.883(19)	1.87(3)	2.72(2)	161(4)
		3·PrOH^{C}		
N1–H1A···O9	0.88	2.05	2.615(8)	121.2
N5–H5A···O1S	0.88	1.84	2.680(19)	159.4
N6–H6A···O2	0.88	2.26	2.70(2)	157.6
N10–H10A···O5	0.88	1.90	2.774(9)	170.4
		4·”PrOH”		
N1–H1A···O9	0.88	2.02	2.593(8)	121.7
N5–H5B···O10	0.88	1.97	2.567(7)	123.5
N6–H6B···O2	0.88	1.77	2.945(15)	167.4
N10–H10A···O5	0.88	1.90	2.767(9)	170.2

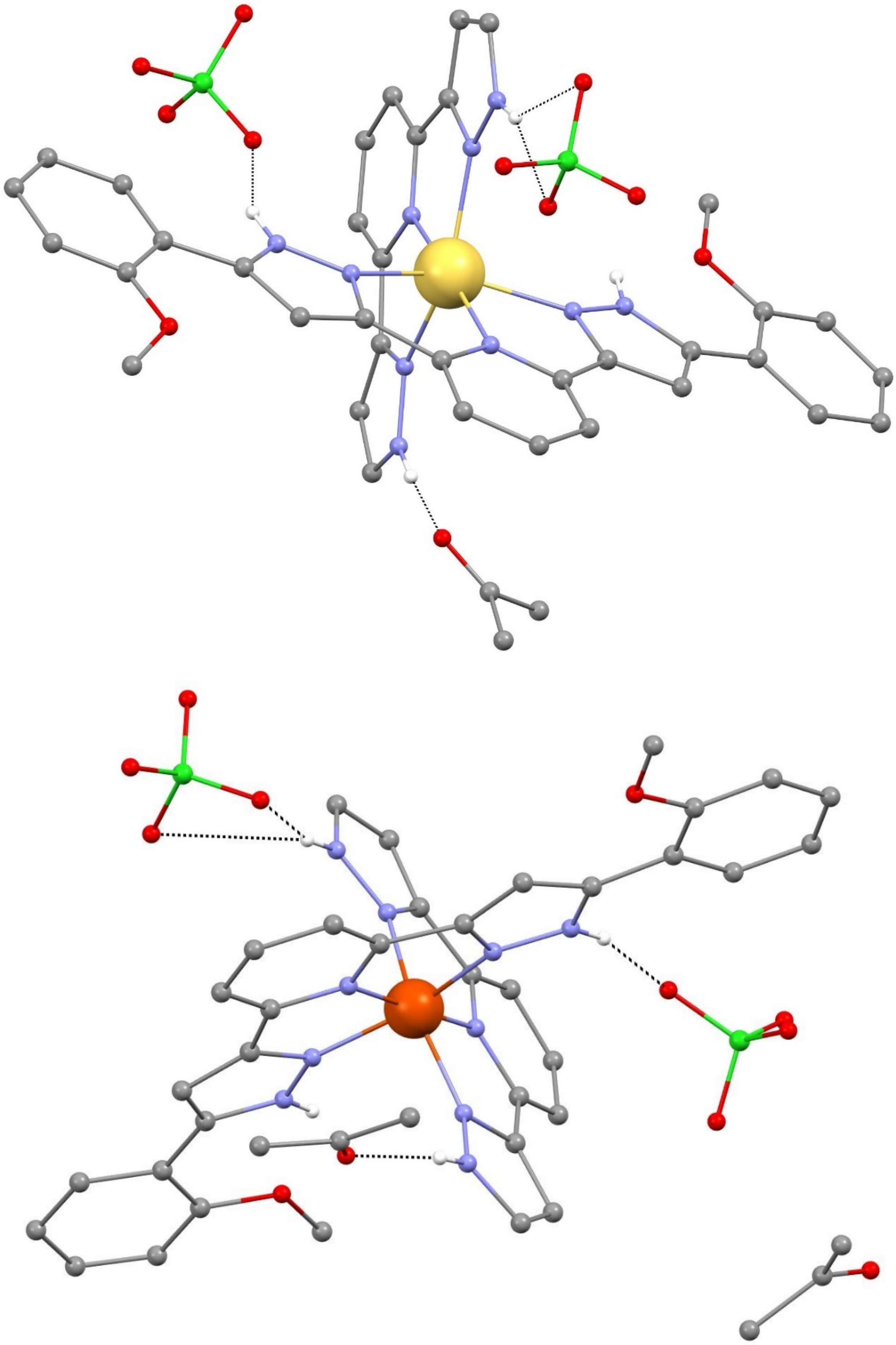

Figure S1. Representation of the asymmetric unit of **1**·Ac (top) and **2**·Ac (bottom). Large ball, Fe; red, O; grey, C; purple, N; green, Cl; white, H. Only hydrogen atoms bound to nitrogen atoms are shown. Only one component of the disordered molecule of acetone in **1**·Ac displayed. Hydrogen bridges are shown as dashed lines.

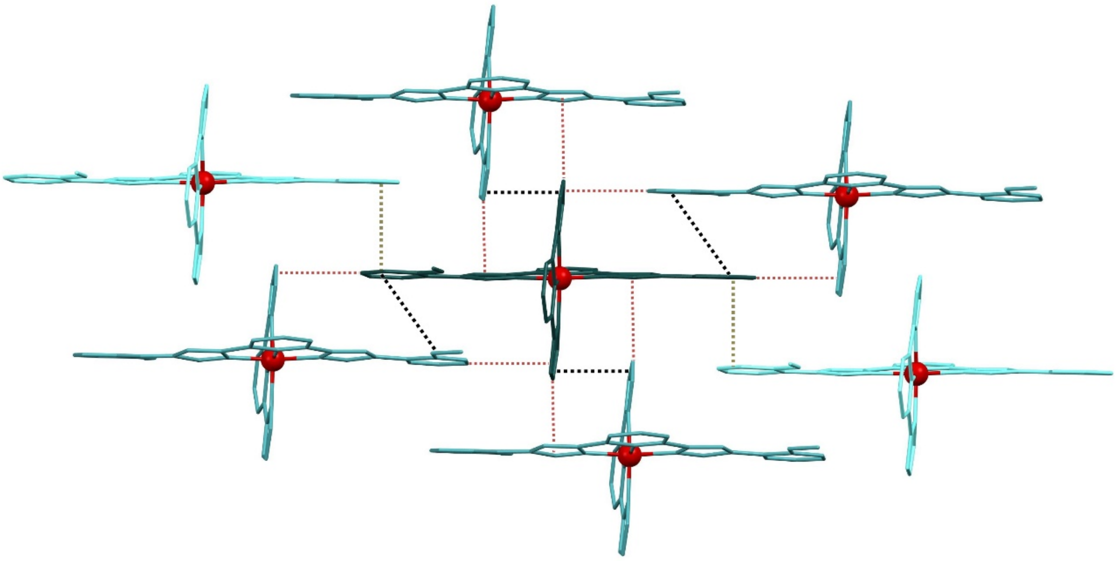

Figure S2. Representation of one complex cation (darkest color) [Fe(bpp)(H$_2$L)]$^{2+}$ of **1**·Ac, which is common to compounds **1**·*solv* to **4**·*solv* (*solv.*; solvate molecule). The intermolecular interactions formed with its four first neighbours (medium dark color) and with its two second neighbours (lightest color) are shown as dashed lines. The interactions with the first neighbours are π···π (black) and C–H···π (red) whereas these with second neighbours are only π···π (brown).

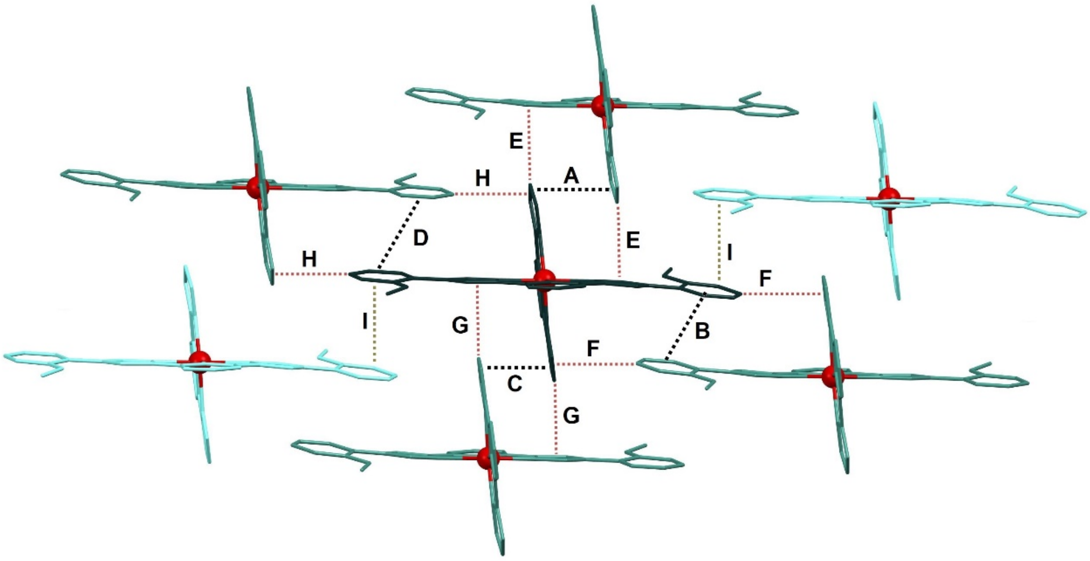

Figure S3. Representation the intermolecular interactions with labels of the complex cation [Fe(bpp)(H$_2$L)]$^{2+}$ of **2**·Ac with its first and second neighbours, shown as dashed lines. The color codes are the same as in Fig. S2.

Table S2. Metric parameters of the intermolecular interactions within **2**·Ac, as distances between closest inter-ring non-H atoms for *π*···*π* interactions and distance between H-atom and adjacent pyrazol centroid for C-H···*π* interactions.

Contact	**Type**	**Distance (Å)**
A	*π*···*π*, pz···pz	3.498(5), N6···C26
B	*π*···*π*, pz···ph	3.616(5), C22···N5
C	*π*···*π*, pz···pz	3.512(4), N10···C36
D	*π*···*π*, pz···ph	3.633(5), C6···C7
I	*π*···*π*, ph···ph	3.981(6), C3···C23
E	C-H···*π*	2.723, C26-H26A···pz
F	C-H···*π*	2.867, C22-H22A···pz
G	C-H···*π*	2.478, C36-H36A···pz
H	C-H···*π*	3.586, C4-H4A···pz

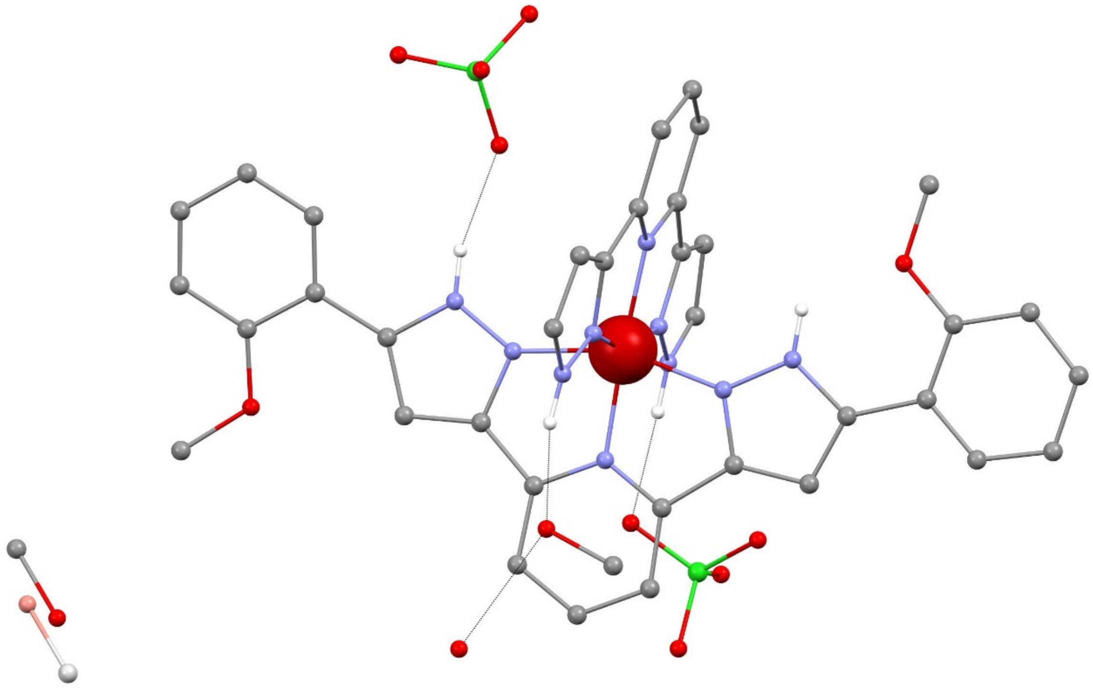

Figure S4. Representation of the asymmetric unit of **3**·MeOH. Large red ball, Fe; red, O; grey, C; purple, N; green, Cl; white, H. Only hydrogen atoms bound to nitrogen atoms are shown. Both components of the disordered molecule of MeOH displayed with full and faded colours, respectively. Hydrogen bridges are shown as dashed lines.

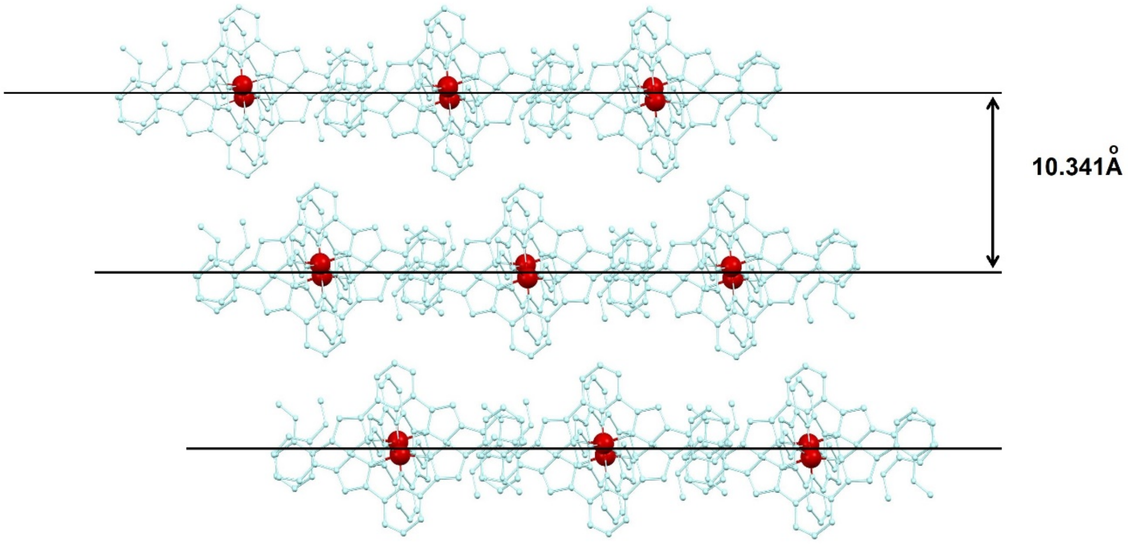

Figure S5. Side view of the parallel sheets made by the complexes from **3**·MeOH, emphasizing the distance between them.

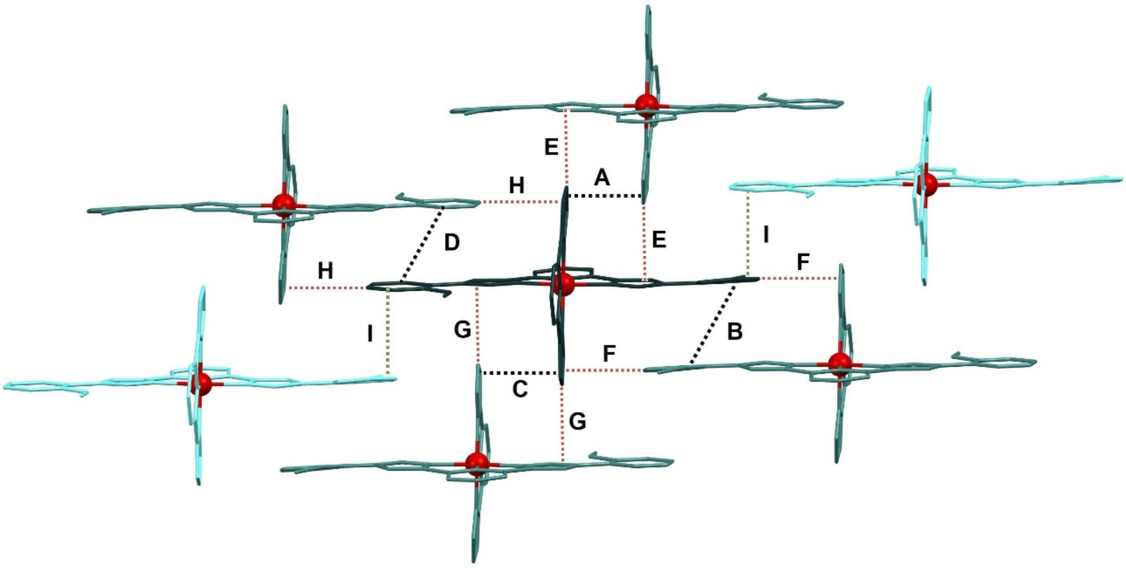

Figure S6. Representation the intermolecular interactions with labels of the complex cation $[Fe(bpp)(H_2L)]^{2+}$ of **3**·MeOH with its first and second neighbours, shown as dashed lines. The color codes are the same as in Fig. S2.

Table S3. Metric parameters of the intermolecular interactions within **3**·MeOH, as distances between closest inter-ring non-H atoms for *π*···*π* interactions and distance between H-atom and adjacent pyrazol centroid for C-H···*π* interactions.

Contact	Type	Distance (Å)
A	*π*···*π*, pz···pz	3.288(5), N6···C26
B	*π*···*π*, pz···ph	3.541(5), C22···N5
C	*π*···*π*, pz···pz	3.576(4), N10···C35
D	*π*···*π*, pz···ph	3.558(5), C1···C6
I	*π*···*π*, ph···ph	3.742(6), C2···C22
E	C-H···*π*	2.436, C26-H26A···pz
F	C-H···*π*	2.905, C22-H22A···pz
G	C-H···*π*	3.314, C35-H35A···pz
H	C-H···*π*	2.716, C3-H3A···pz

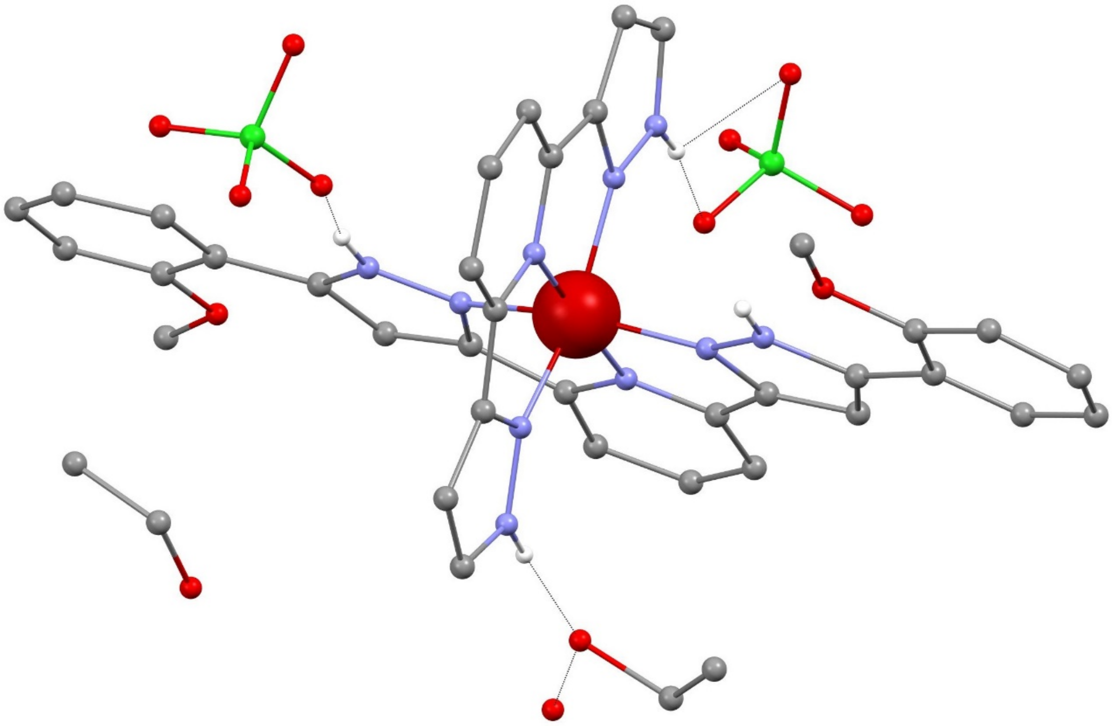

Figure S7. Representation of the asymmetric unit of **3**·EtOH. Large red ball, Fe; red, O; grey, C; purple, N; green, Cl; white, H. Only hydrogen atoms bound to nitrogen atoms are shown. Hydrogen bridges are shown as dashed lines. The molecule of H_2O is shown only as an O-atom. This molecule and that of EtOH not involved in H-bonding present 50% occupancy.

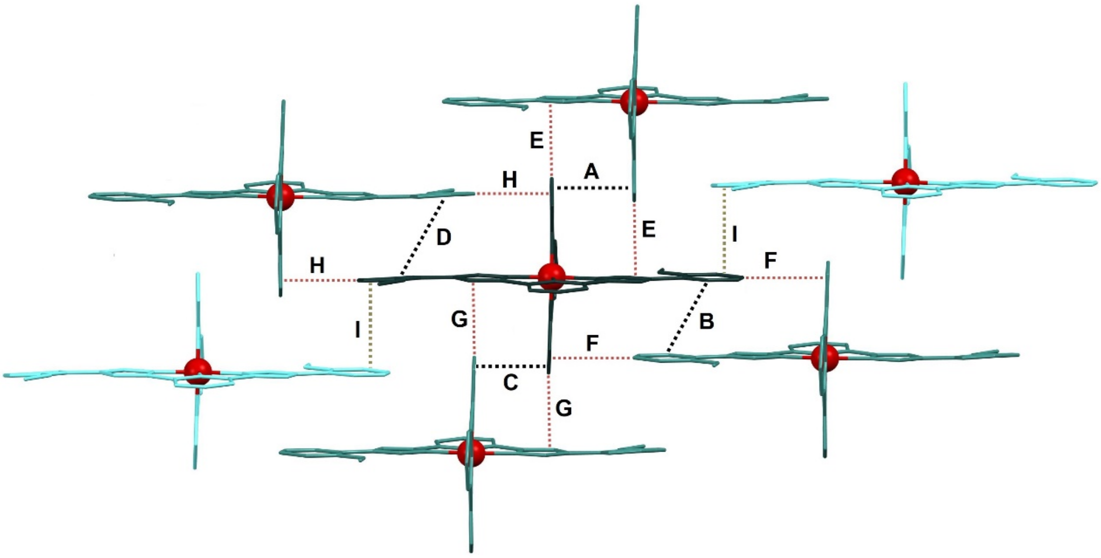

Figure S8. Representation the intermolecular interactions with labels of the complex cation $[Fe(bpp)(H_2L)]^{2+}$ of **3**·EtOH with its first and second neighbours, shown as dashed lines. The color codes are the same as in Fig. S2.

Table S4. Metric parameters of the intermolecular interactions within **3**·EtOH, as distances between closest inter-ring non-H atoms for *π*···*π* interactions and distance between H-atom and adjacent pyrazol centroid for C-H···*π* interactions.

Contact	Type	Distance (Å)
A	*π*···*π*, pz···pz	3.560(5), C35···C36
B	*π*···*π*, pz···ph	3.614(5), C2···C7
C	*π*···*π*, pz···pz	3.354(4), N6···C26
D	*π*···*π*, pz···ph	3.567(5), C19···C18
I	*π*···*π*, ph···ph	3.771(6), C2···C22
E	C-H···*π*	3.165, C35-H35A···pz
F	C-H···*π*	2.779, C3-H3A···pz
G	C-H···*π*	2.475, C26-H26A···pz
H	C-H···*π*	2.996, C22-H22A···pz

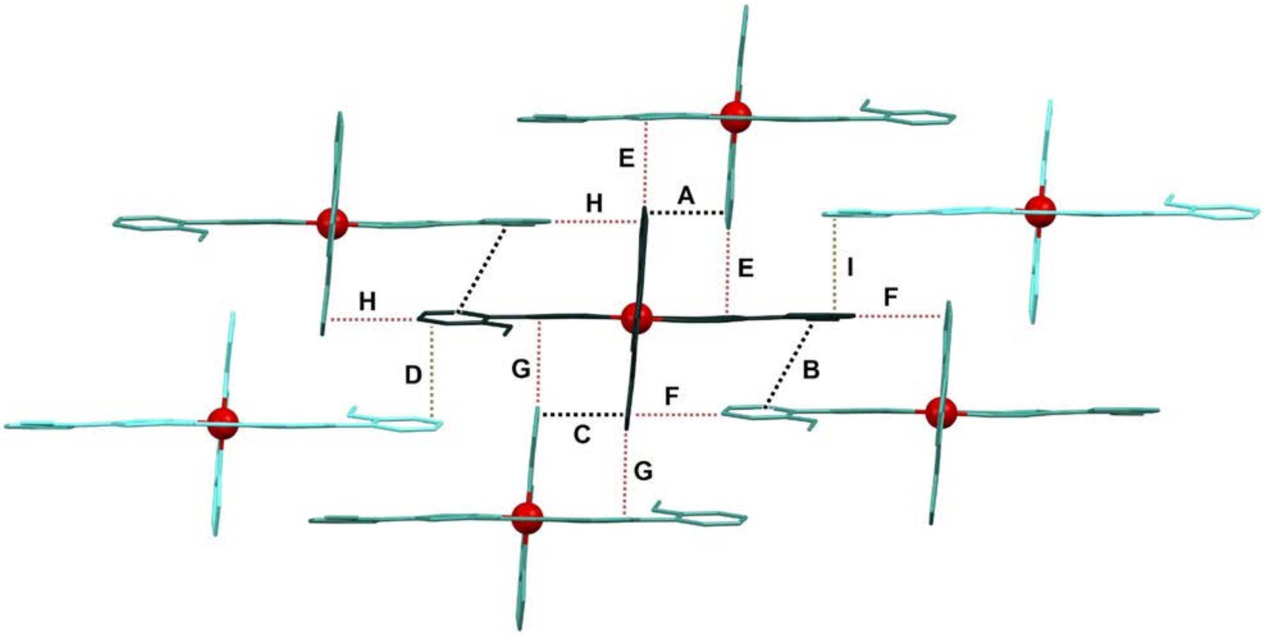

Figure S9. Representation the intermolecular interactions with labels of the complex cation $[Fe(bpp)(H_2L)]^{2+}$ of **3**·PrOH with its first and second neighbours, shown as dashed lines. The color codes are the same as in Fig. S2.

Table S5. Metric parameters of the intermolecular interactions within **3**·PrOH^A, as distances between closest inter-ring non-H atoms for $\pi\cdots\pi$ interactions and distance between H-atom and adjacent pyrazol centroid for C-H$\cdots\pi$ interactions.

Contact	Type	Distance (Å)
A	$\pi\cdots\pi$, pz···pz	3.297(4), C26···N6
B	$\pi\cdots\pi$, pz···ph	3.560(5), C24···C8
C	$\pi\cdots\pi$, pz···pz	3.390(4), C35···C36
D	$\pi\cdots\pi$, ph···ph	3.760(5), C3···C4
I	$\pi\cdots\pi$, ph···ph	3.872(5), C24···C22
E	C-H$\cdots\pi$	2.788, C26-H26A···pz
F	C-H$\cdots\pi$	2.663, C4-H4A···pz
G	C-H$\cdots\pi$	3.416, C35-H35A···pz
H	C-H$\cdots\pi$	2.991, C22-H22A···pz

TGA EXPERIMENTS

Thermogravimetric analyses (TGA) of compounds **3**·MeOH, **3**·EtOH and **3**·PrOH reveal a weight lost upon heating, of 6.2/7.0/6.2 %, leading to **4**·”MeOH”, **4**·”EtOH” and **4**·”PrOH”, respectively. This is the result of total depletion of solvate molecules for **4**·”MeOH” (1.25MeOH+0.5H_2O represents 5.2%; the discrepancy is likely due to previous absorption of moisture from air) and for **4**·”PrOH” (1PrOH is 6.3%). For **4**·”EtOH”, the weight loss corresponds to desorption of only ethanol (1.5EtOH corresponds to 7.1 %), with H_2O likely remaining in the lattice. This differing desorption pattern explains a completely different magnetic behavior than observed for **4**·”MeOH” and **4**·”PrOH”.

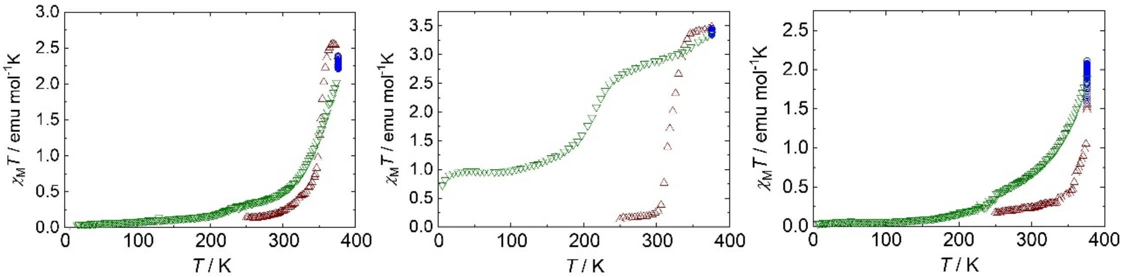

Figure S10. Plots of $\chi_M T$ *vs* T for microcrystalline samples of **3**·MeOH (top), **3**·EtOH (middle) and **3**·PrOH (bottom) when successively, *i*) heating from 250 to 375 K (wine color), *ii*) maintaining the temperature for 375 K (blue), and *iii*) cooling from 375 to 5 K (olive color).

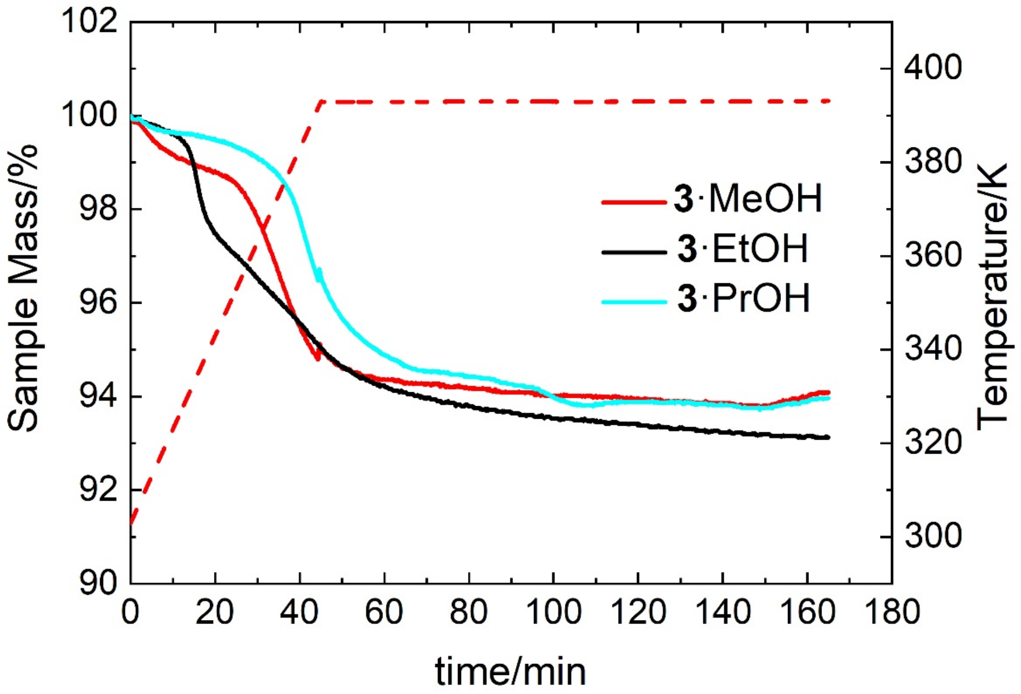

Figure S11. TGA analysis of **3**·MeOH, **3**·EtOH and **3**·PrOH, represented as the evolution in time of the normalised sample mass, upon heating from room temperature to 393 K and then maintaining constat the temperature. The broken red line shows the change of temperature with time.

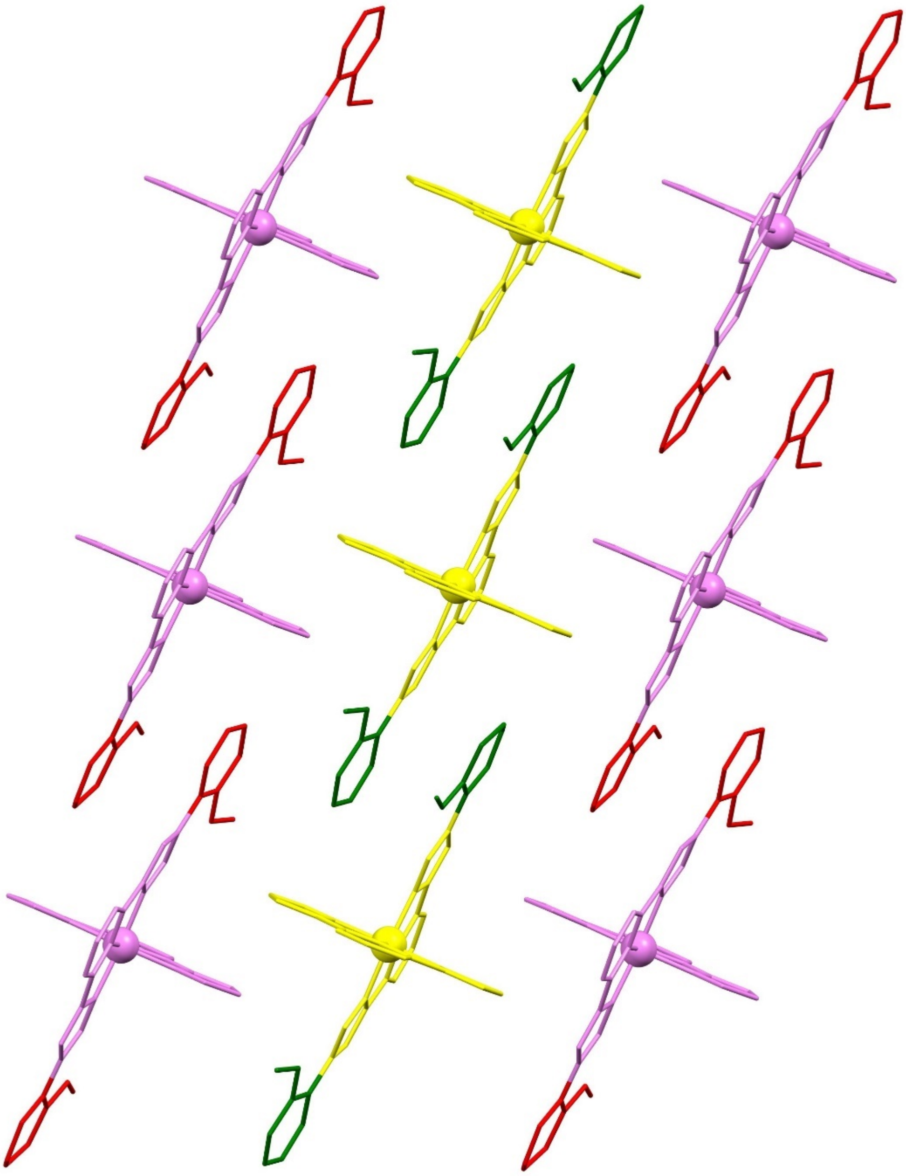

Figure S12. Arrangement of the $[Fe(bpp)(H_2L)]^{2+}$ complexes of **3**·PrOH^{C} as sheets within the lattice. Yellow and violet colors represent their two possible orientations as a function of the H_2L and bpp positions with respect to the plane of the sheets. Green and red denote the orientation of the methoxy groups of H_2L with respect to this plane (upwards and downwards, respectively).

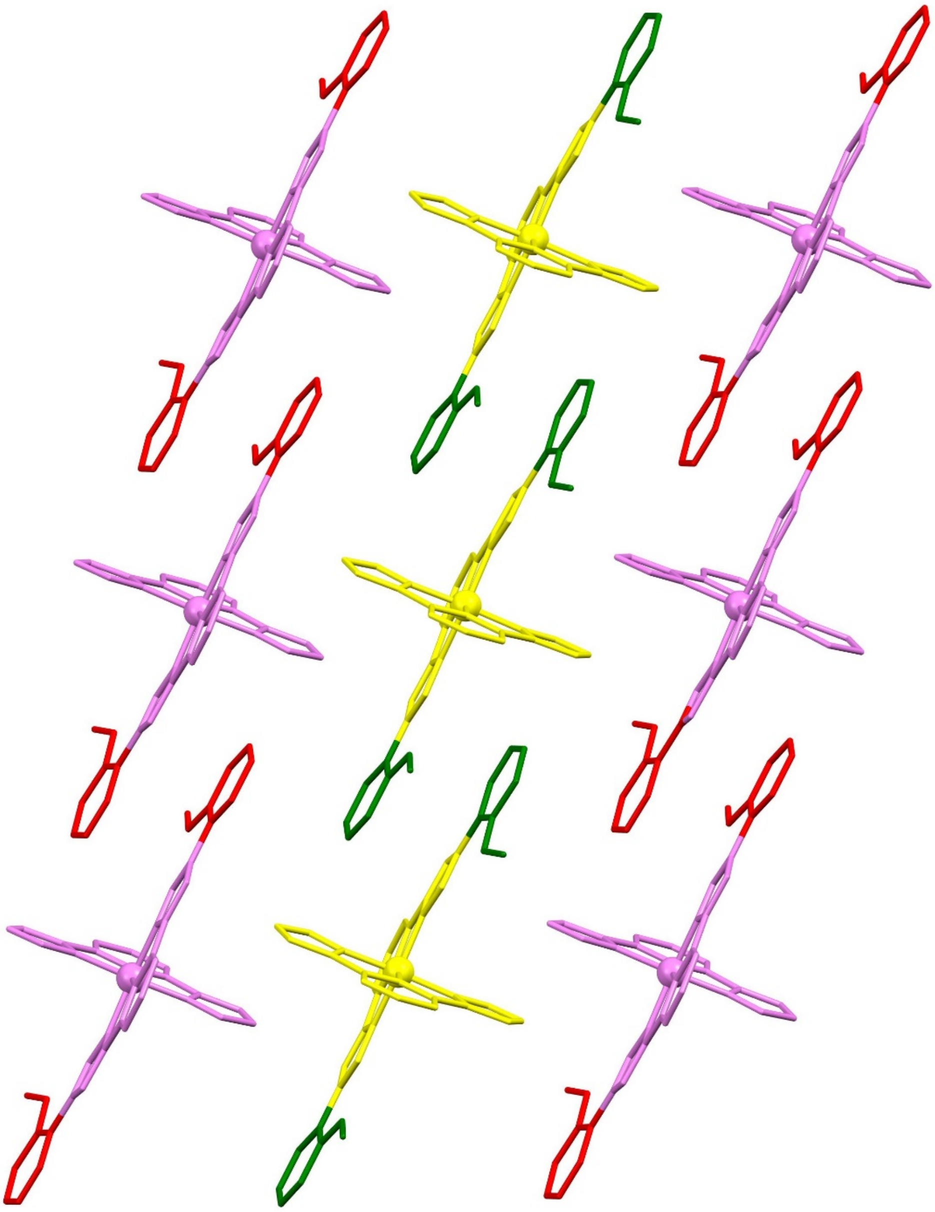

Figure S13. Arrangement of the [Fe(bpp)(H_2L)]$^{2+}$ complexes of **4**·”PrOH” as sheets within the lattice. The same color code as in Fig. S12 has been used.

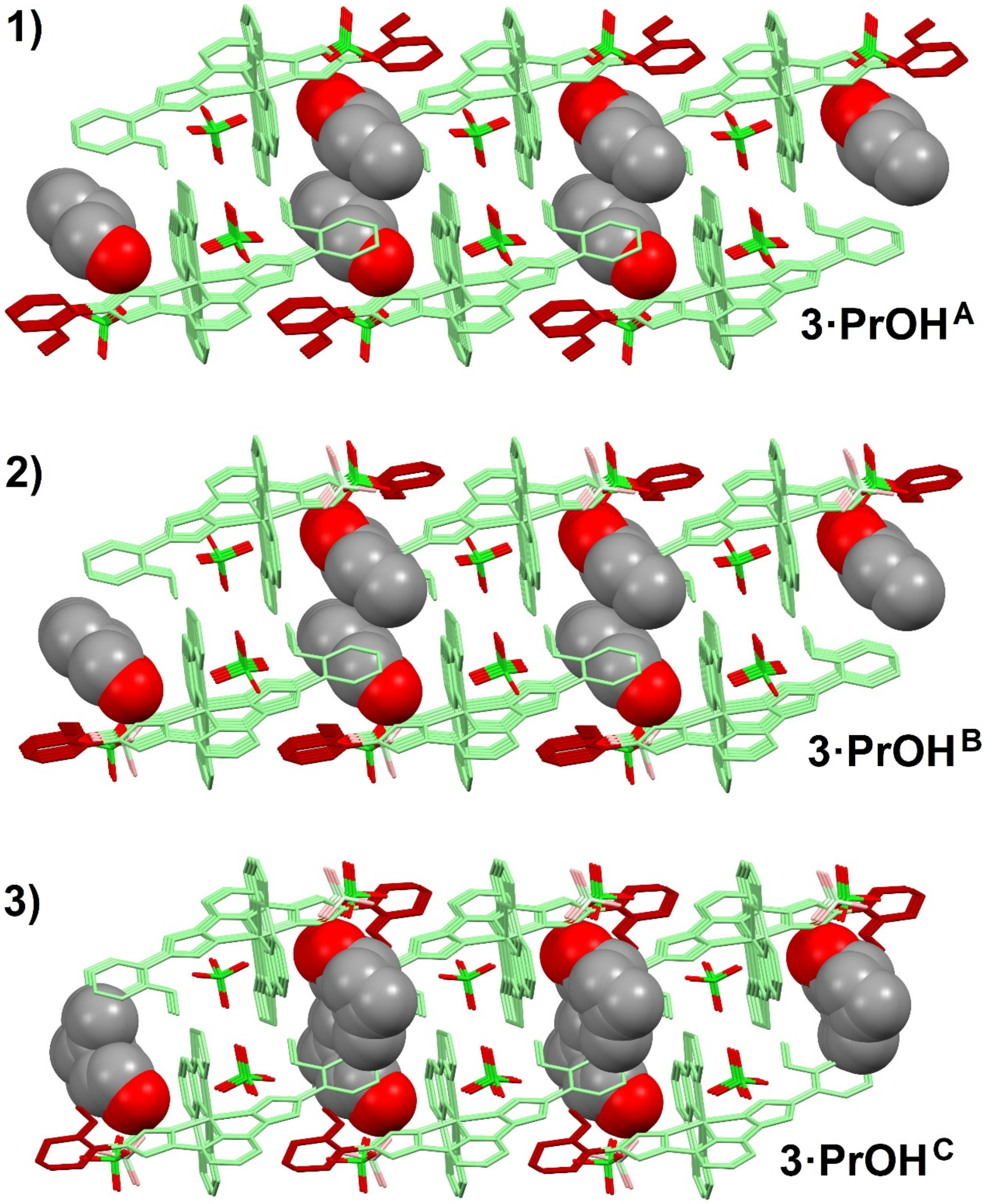

Figure S14. View of the lattices of **3**·PrOH^{A} (1), **3**·PrOH^{B} (2) and **3**·PrOH^{C} (3), approximately down the crystallographic axis '*a*', along the proposed pathway followed by the PrOH molecules to migrate. Complexes are green, except the methoxyphenyl ring that has been shown by SCXRD to rotate (in red). The PrOH molecules are emphasized in the space-filling style. ClO_4^- ions are in red (O) and green (Cl), with the second disordered component (when applicable) faded.